Journal Pre-proof

Activated H_2O_2 on Ag/SiO_2–$SrWO_4$ surface for enhanced dark and visible-light removal of methylene blue and *p*-nitrophenol

Hamdy S. El-Sheshtawy, Zaynab ghubish, Kamel R. Shouir, Maged El-Kemary

PII: S0925-8388(20)32212-X

DOI: https://doi.org/10.1016/j.jallcom.2020.155848

Reference: JALCOM 155848

To appear in: *Journal of Alloys and Compounds*

Received Date: 24 February 2020

Revised Date: 24 May 2020

Accepted Date: 28 May 2020

Please cite this article as: H.S. El-Sheshtawy, Zaynab ghubish, K.R. Shouir, M. El-Kemary, Activated H_2O_2 on Ag/SiO_2–$SrWO_4$ surface for enhanced dark and visible-light removal of methylene blue and *p*-nitrophenol, *Journal of Alloys and Compounds* (2020), doi: https://doi.org/10.1016/j.jallcom.2020.155848.

Hamdy S. El-Sheshtawy and Zaynab ghubish conceived of the presented idea and performed experiments

Hamdy S. El-Sheshtawy and Kamel R. Shouir developed the idea

Maged El-Kemary supervised the findings of this work. All authors discussed the results and contributed to the final manuscript.

Activated H_2O_2 on Ag/SiO_2-$SrWO_4$ Surface for Enhanced Dark and Visible-light Removal of Methylene Blue and *p*-nitrophenol

Hamdy S. El-Sheshtawy[1*], Zaynab ghubish[2], Kamel R. Shouir[2], Maged El-Kemary[2]

[1]Chemistry Department, Faculty of Science, Kafrelsheikh University, Kafrelsheikh, Egypt

[2]Institute of Nanoscience and Nanotechnology, Kafrelsheikh University, Kafrelsheikh, Egypt

Abstract

Activated H_2O_2 on the surface of nanostructures for advanced oxidation process attracts the interest for energy consumption, time saving rather than Fenton reaction process. Here, we introduce Ag/SiO_2 NPs immobilized on $SrWO_4$ surface for enhanced catalytic and photocatalytic oxidation of methylene blue and reduction of *p*-nitrophenol by H_2O_2 surface activation. Both theoretical calculations (rwb97xd/LANL2DZ) and experimental (FT-IR and XRD) show that the catalytic enhancement was due to the surface interaction between Ag/SiO_2 and $SrWO_4$ that activate H_2O_2 surface molecules in absence of light. The photocatalytic enhancement was interpreted by the hot electrons ejected from Ag NPs to the $SrWO_4$ rather than the p-n junction created by Ag/SiO_2 and $SrWO_4$ mechanism. Different spectroscopic techniques such as SEM, TEM, XRD were used for the catalysts characterizations. The optical measurements such as UV-Vis and photoluminescence were incorporated to further support the mechanism. The catalyst posses high catalytic activity over wide pH range (4-10).

Keywords: activated H_2O_2; $Ag/SiO_2/SrWO_4$; catalytic; photocatalytic; DFT calculations

Corresponding author e-mail: hamdyalfy@gmail.com

1. Introduction

Although several methods have been developed for water treatment such as membrane filtration [1], advanced oxidation [2], catalytic/photocatalytic degradation, Fenton reaction persists as the most effective oxidation method. This was due to the high yield of •OH radical and fast Fe^{2+}/Fe^{3+} cycle. However, it still suffer from some drawbacks such as limitation to the acidic pH and environmental concern related to release of toxic iron ions [3]. Hence, Fenton-like reaction has been developed to overcome such defects using metal ions, metal oxides, nanocomposites and acids [4-7]. Here, the reaction initiated by an external stimulus such as light illumination to induce oxidation state change and/or charge separation process. In addition, the H_2O_2 decomposition could be improved by the adsorption and interaction with the surface of the catalyst to enhance the liberation of reactive oxygen species [8-10].

$SrWO_4$ was extensively investigated and integrated in different applications such optoelectronic devices, laser-state systems, energy storage material, and photocatalysts [11-14]. However, $SrWO_4$ suffer from the low absorption coefficient particularly in the visible light region, and the high electron/hole recombination process [14,15]. In order to enhance the photocatalytic properties of $SrWO_4$, different methods were used such as doping with metal ions [16], or immobilization over graphene sheets [14].

Silver nanoparticles (AgNPs) have attracted the interest of researchers because of the fascinating properties both in dark and under visible light. In absence of light, AgNPs could activate the production of reactive oxygen species (ROS) such as hydroxyl radical (•OH), superoxide radical (O_2^{-}•) and singlet oxygen ($^1O_2$) [17,18]. ROS is the prominent factor in antimicrobial and antibacterial agents [19,20]. Thus, AgNPs is a well known bactericidal agent by breakdown of the membrane wall and DNA damage [21]. On the other hand, when AgNPs illuminated with suitable light wavelength (visible light) the surface electrons oscillate to inaugurate the surface plasmon resonance (SPR) effect. SPR increases the ability of AgNPs

for absorbing the visible light, which subsequently delivers to wide-band gap semiconductor in order to boost the charge separation.

In this work, we introduce Ag/SiO_2 on $SrWO_4$ surface as an activator for H_2O_2 in absence and presence of visible light. The embedded Ag NPs on solid support such as SiO_2 are formed by ion implantation, which effectively prevents Ag from aggregation or oxidation through direct contact with $SrWO_4$ [22-24]. The doped Ag NPs enhance the visible light absorption of $SrWO_4$ and decreases the band gap through the surface plasmon effect. Hence, the intimate contact between Ag NPs and $SrWO_4$ boosted the generation of •OH and O_2^{-}• that highly increase the MB degradation and *p*-nitroaniline removal. The structures of the catalysts were investigated by different techniques such as XRD, TEM, SEM, UV-Vis, and photoluminescence. DFT calculations (*r*wb97xd/LANL2DZ) corroborated the experimental results for the interactions between Ag NPs and $SrWO_4$.

2. Materials and Methods

2.1 Materials:

The starting materials used in this work were of analytical grade. Metal salts, strontium nitrate anhydrous, sliver nitrate, poly vinyl alcohol, cetyltrimethylammonium bromide (CTAB) were obtained from Sigma-Aldrich (Germany). All the chemicals were used without further purification.

2.2 Preparation of Ag/SiO_2 core shell

Silver nanoparticles was prepared by adding 0.25 mM of silver nitrate to solution of sodium borohydride (0.025 mM) dissolved in polyvinyl alcohol (20 ml) as a capping agent. The solution was then stirred (2000 rpm) at room temperature for 2 hours. The product was extracted using a rotary evaporator at the 70 ^{0}C [25,26]. Then, 0.01 g from the dry Ag NPs

was dispersed in 20 ml distilled water and stirred for 5 min at room temperature. SiO_2 NPs (0.1 g) was then added and further stirred until the yellow suspension was observed. The product was separated by centrifuge (6000 rpm), washed with distilled water (3 x 20 ml) and ethanol (3 x 10 ml) and dried in air at 80 ^oC for 24 h [27].

2.3 Preparation of $SrWO_4$

0.005 mole of $Sr(NO_3)_2$ and 0.005 mole of $NaWO_4$ were separately dissolved in 15.00 mL of ethylene glycol (PEG-6000). The two solutions were mixed with continuous stirring (rpm=2400) for 24 h at room temperature (30 ^oC). Finally, white precipitate was obtained and washed with distilled water (3 x 20 ml) and ethanol (3 x 10 ml). The product was dried in air at 80 ^oC for 24 h [14].

2.4 Preparation $Ag/SiO_2/SrWO_4$

$Ag/SiO_2/SrWO_4$ nanocomposite was obtained by dispersing 100 mg of Ag/SiO_2 and 300 mg of $SrWO_4$ in ethylene glycol (50 ml) to maintain the required Ag NPs percent. In order to maintain the homogeneity of the nanoparticles, the solution was stirred for 24 h at room temperature (30 ºC). The pH of the solution kept constant at 4.6 using HCl or NaOH aqueous solution. Then the product was separated by centrifuge (6000 rpm) and washed three times with distilled water (3 x 20 ml) and ethanol (3 x 10 ml). To completely remove the ethanol, the sample was kept in the oven for 24 hours at 70 ºC.

2.5 Catalytic and Photocatalytic removal of MB

20 mg of the catalyst (Ag/SiO_2, $SrWO_4$, and $Ag/SiO_2/SrWO_4$) was dispersed in 10 ml of an aqueous solution of MB (10 ppm) at room temperature. The mixture solution was stirred in the dark for 30 min to reach the adsorption/desorption equilibrium. For catalytic experiment, 0.08 M H_2O_2 was added and the concentration of MB was recorded by UV-Vis spectrophotometer. In case of photocatalytic experiment, after the 0.08 M of H_2O_2 addition, the solution was irradiated by visible light (500 W tungsten halogen lamp with $\lambda > 420$ nm).

2.6 Photoreduction of *p*-nitrophenol

The photoreduction of *p*-nitrophenol (NP) was performed under visible light irradiation and room temperature. 40 μL NP (0.01 M) was mixed with deionized water (2.8 ml) and stirred for 1hr to establish equilibrium. Then, 80 μL of $NaBH_4$ solution (0.5 M) were added to evolve bright yellow color. Subsequently, 10 μL of the catalyst (5 mg/ml) was added and the yellow color disappear was monitored with UV-Vis spectrophotometer at 440 nm.

2.7 Characterization

The particle size and shape of nanocomposites were characterized by transmission electron microscopy (TEM, JEM-2100 (JEOL). The morphology of the fabricated nanostructures scanning electron microscope (SEM, JEOL-IT100LA) The XRD patterns were recorded using Shimadzu X-ray diffractometer with CuKa1 radiation (k = 1.54056 Å). The accelerating voltage of 40 kV and an emission current of 30 mA were used. The FT-IR spectra were recorded using JASCO- FT-IR 6800 spectrometer. The Photoluminescence emission spectra were recorded at room temperature with a spectrofluorometer Shimaduz RF5301PC. UV visible were recorded by Shimadzu 240 instrument. Total organic carbon (TOC) was measured using a Sievers 5310 C analyzer and experiments were performed three times.

3- Results and Discussion

The crystal structure of the prepared nanoparticles was investigated by XRD spectroscopy (Fig. 1a). The XRD pattern of Ag NPs shows the characteristic peaks at locate at 37.76, 43.76, 64.41, 77.61 related to (111), (200), (220), and (311) respectively, which is identical to JCPDS No.87-0720. Deposition of Ag NPs on the SiO_2 NPs reflected on the XRD pattern of Ag/SiO_2 pattern, which show an extra broad scattering peak for the amorphous SiO_2 [28] in addition to the Ag NPs peaks. Similarly, $SrWO_4$ NPs show an XRD pattern identical to the scheelite tetragonal structure phase with the characteristic peaks at 17.51, 27.12, 29.45, 32.85, 44.93, 46.93, 51.40, 55.45, 57.15 related to (101), (112), (004), (200), (204), (220), (116),

(312), (224) crystal plane $SrWO_4$ corresponds to JCPDS No. 08-0490. The XRD pattern of $Ag/SiO_2/SrWO_4$ nanocomposite show the combination of the individual peaks of the components with lower Ag NPs peaks intensities at 37.7, 43.7, 64.4, and 77.6°. The decrease of peaks intensities reflects the strong interaction between Ag/SiO_2 and $SrWO_4$.

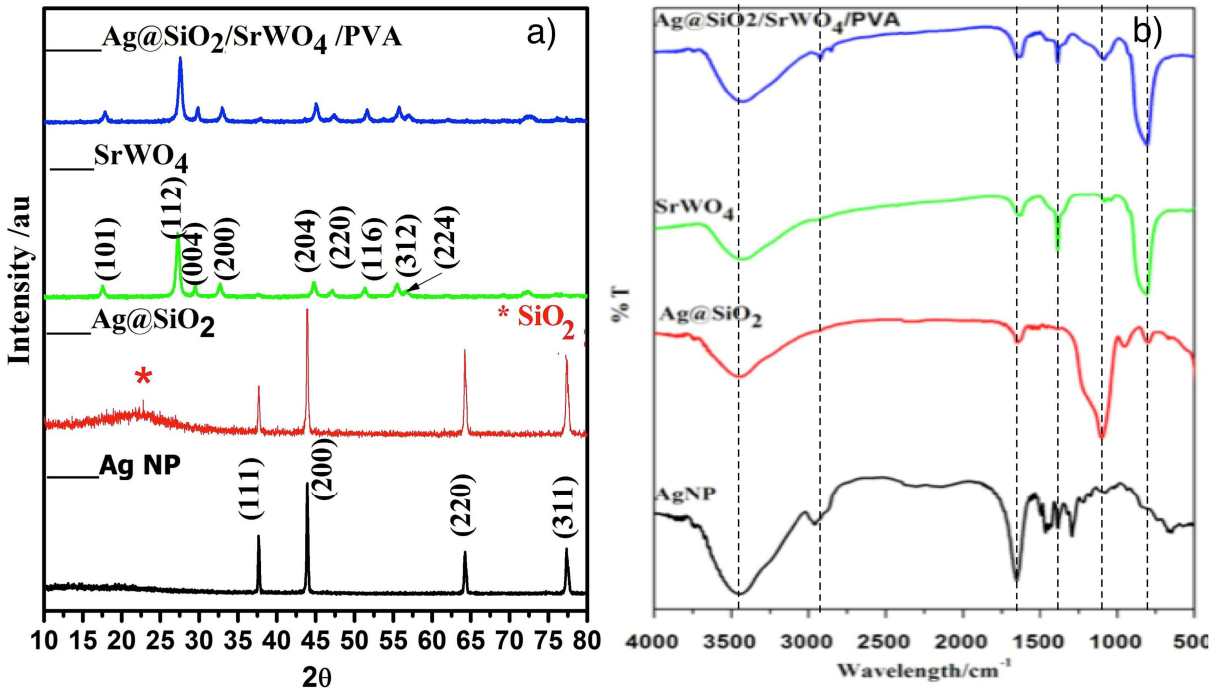

Fig. 1: a) XRD pattern and b) FT-IR spectra of Ag NPs, Ag/SiO_2, $SrWO_4$, and $Ag/SiO_2/SrWO_4$.

The FT-IR spectrum of Ag NPs shows a broad peak at 3400 cm^{-1} characteristic for the presence of hydroxyl surface groups (OH^-) (Fig. 1b). Aliphatic CH groups appeared at 2800 cm^{-1} in addition to the stretching C-C bond at 1730 cm^{-1}. Deposition of Ag NPs on the SiO_2 NPs causes the decrease of the OH and C-C peaks due to the strong surface interaction. The enhanced intensity of 1100 cm^{-1} peak was assigned to the Ag/SiO_2 strong interaction through O-Si-O bond. On the other hand, $SrWO_4$ show the characteristic peak at 805 cm^{-1} for the antisymmetric stretching vibration of O-W-O bond in WO_4^{-2} anions [29]. Upon addition of Ag/SiO_2 to the $SrWO_4$ NPs, the spectrum shows the combined peaks with the decrease of

intensity of 1100 cm^{-1} of Ag/SiO_2 and peak at 805 cm^{-1} of $SrWO_4$, which could be interpreted by the strong interaction between Ag/SiO_2 and $SrWO_4$.

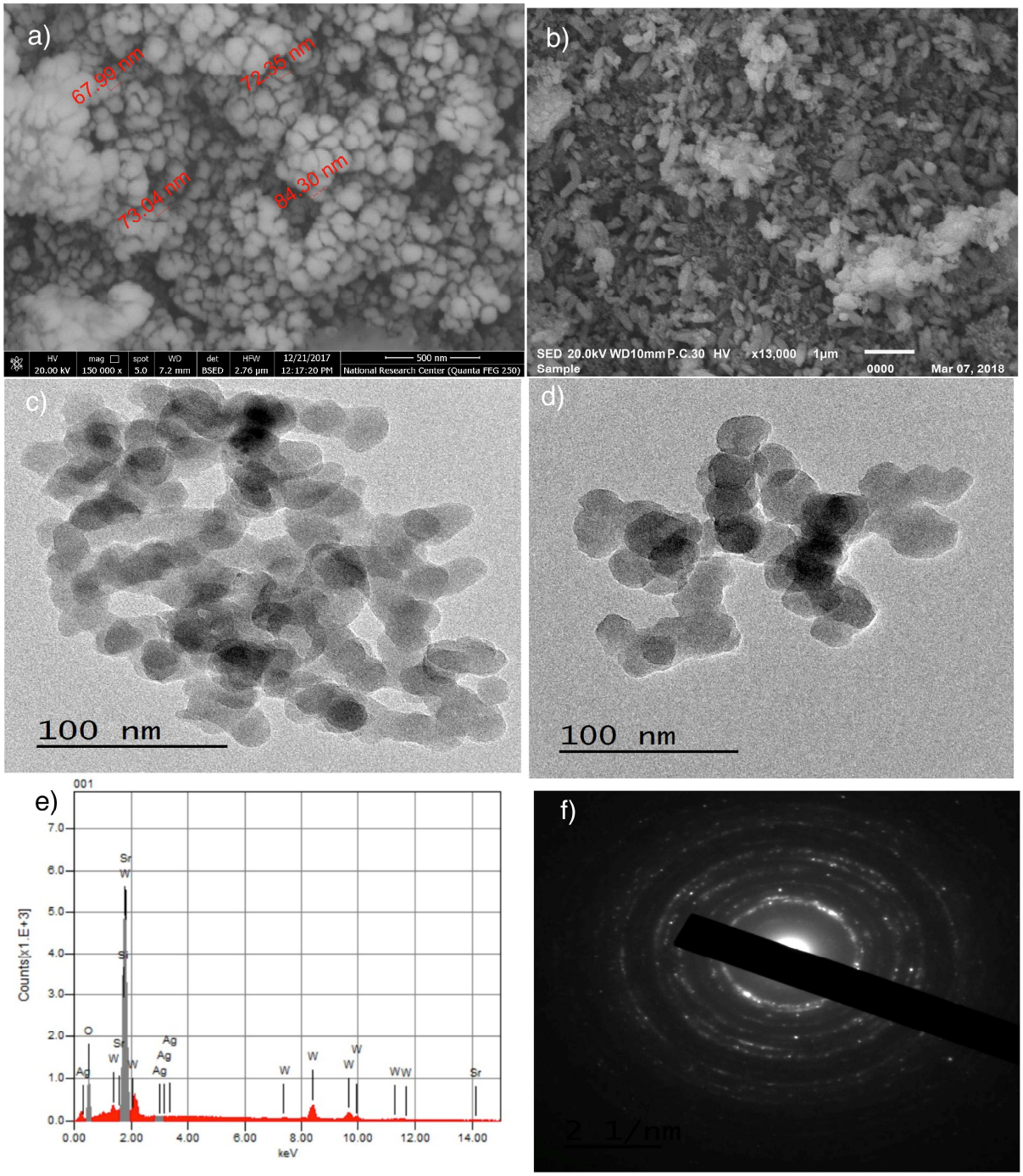

Fig. 2: SEM for a) Ag-SiO_2, b) $Ag/SiO_2/SrWO_4$ and TEM of c) Ag/SiO_2, d) $Ag/SiO_2/SrWO_4$. The EDS of $Ag/SiO_2/SrWO_4$ e) and scattered pattern in f).

The morphology of the nanocomposites was explored using both SEM and TEM (Fig. 2). The data show that Ag NPs and Ag/SiO_2 nanosphere posses an average size of 8 nm and 70 nm respectively. Upon addition of Ag/SiO_2 to $SrWO_4$, the average size of $Ag/SiO_2/SrWO_4$ slightly increased to 75 nm. This result was confirmed by the TEM (Fig 2c-d). The composition of the nanocatalyst was determined from the EDS (Fig. 2d). As shown, the EDS indicate the presence of the individual component of $Ag/SiO_2/SrWO_4$. The Ag NPs percentage was measured as of 3.5% in $Ag/SiO_2/SrWO_4$ by EDS, which was confirmed by ICP-AES technique. In addition the crystalline nature of the catalyst was observed from the presence of the scattered pattern (Fig 2f).

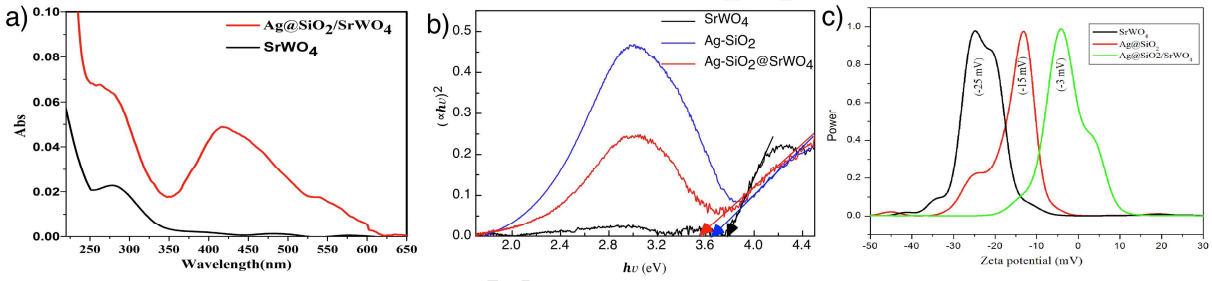

Fig. 3: a) absorption spectrum of $Ag/SiO_2/SrWO_4$, b) Tauc plot and c) surface charge for $SrWO_4$, Ag/SiO_2 and $Ag/SiO_2/SrWO_4$ nanocomposite.

The UV-Vis absorption spectra of $SrWO_4$ and $Ag/SiO_2/SrWO_4$ were measured (Fig.3a) in aqueous solution. The absorption spectra of $SrWO_4$ give peak at 280 nm, while $Ag/SiO_2/SrWO_4$ shows an extra broad peak at 420 nm attributed to the Ag NPs plasmonic absorption. The optical band gap of the $SrWO_4$, Ag/SiO_2 and $Ag/SiO_2/SrWO_4$ was calculated from the UV-visible diffuse reflectance measurements [14]. Kubelka-Munk function, $\alpha h\nu = A(h\nu - E_g)^2$, where a, h, ν, A, *and* E_g are absorption coefficient, Planck constant, light frequency, constant and band gap energy respectively. To obtain the band gap energy, $(\alpha h\nu)^{1/2}$ versus the $h\nu$ was plotted and extrapolation of the straight line portion to $h\nu=0$ [30]. Fig 3b shows the optical band gap of $SrWO_4$ at 3.8 eV, and lower value for Ag/SiO_2 (3.67

eV), while $Ag/SiO_2/SrWO_4$ nanocomposite show a lower band gap at 3.56 eV. Interestingly, the optical measurements show the emergence of strong absorption peak at 2.9 eV attributed to deposition of the surface Ag NPs. The surface charge of the catalysts was measured by Zeta potential (Fig. 3c). The high negative surface charge of $SrWO_4$ (–25.0 mV) was decreased with the addition of Ag/SiO_2 (–15.0 mV). In average, relatively low surface charge was situated on $Ag/SiO_2/SrWO_4$ (–3.0 mV), which might be the reason for the wide activity of the catalysts in different pH values (see discussion below).

Catalytic and Photocatalytic activity

The catalytic activity of Ag/SiO_2, $SrWO_4$, and $Ag/SiO_2/SrWO_4$ was investigated using MB as model cationic dye by different methodologies such as UV-Vis, TOC, and in situ FT-IR spectroscopy. In absence of either light or H_2O_2, the catalysts show insignificant adsorption 11.2, 9.7, and 12.1 % for Ag/SiO_2, $SrWO_4$, and $Ag/SiO_2/SrWO_4$, respectively (Fig. 4a, 5a). Upon H_2O_2 addition, Ag/SiO_2 shows 10% degradation efficiency after 40 min (Fig. 4b), while $SrWO_4$ take longer time (70 min) to reach the same degradation efficiency (10%) (Fig.5b). Interestingly, the hybrid $Ag/SiO_2/SrWO_4$ nanocomposite completely decomposes MB in 32 min. Illumination of the MB solution contains Ag/SiO_2 with visible light (λ> 400 nm) decompose 10% of the dye at 40 min (Fig. 4c), while the $SrWO_4$ take longer time (70 min) to achieve the same efficiency (Fig. 5c). The addition of $Ag/SiO_2/SrWO_4$ to the MB solution completely decomposes the dye in 70 min (Fig. 6a).

Illumination of the MB with visible light in presence of H_2O_2 significantly reduces the time for degradation process. For example, Ag/SiO_2 remove about 38.8 % in 20 min while $SrWO_4$ need more than 50 min to remove 18% (Table 1). On the other hand, $1\%Ag/SiO_2/SrWO_4$ initiate the photo-oxidation process of MB to remove more than 90% in 40 min. $3.5\%Ag/SiO_2/SrWO_4$ needs only 22 min to remove more than 99% of the MB (Fig. 6b).

Further increase of the Ag NPs percentage to 5% reduces the photocatalytic activity, which ascribed to the surface agglomeration of Ag NPs at high concentrations.

In order to clarify the mineralization of MB by $Ag/SiO_2/SrWO_4$, the total organic carbon (TOC) was measured before and after the photocatalytic process [31,32]. Before visible light irradiation, the solution of MB and $Ag/SiO_2/SrWO_4$ gives TOC value of 28.2 mg/L. Upon irradiation of the MB solution (20 min) containing 3.5%$Ag/SiO_2/SrWO_4$ (20mg), the TOC value reduced to 2.7 mg/L [33]. This indicates that $Ag/SiO_2/SrWO_4$ potentially convert MB to carbon dioxide and water [34,35]. Further, the FT-IR spectrum of MB show vibrational modes related to the organic molecule structure such as the NH (3340 cm^{-1}), aromatic CH groups (2010-2080 cm^{-1}) (Fig.6c) [36,37]. Fig. 6c shows the disappearing of the complex vibrational modes and decreasing the intensity of the aromatic CH for MB after adding the catalyst and irradiated the solution for 10 min,15 min and 20 min. At the same time increasing intensity peak at 1640 cm^{-1} confirm the formation of H_2O [36]. The vibration peak at 3524 cm^{-1} is assigned to the stretching vibration mode of the surface hydroxyl groups. This peak intensity increases with the irradiation time and MB degradation, which ascribed to the chemisorbed water on the $Ag/SiO_2/SrWO_4$ surface. Hence, both TOC and FT-IR results confirm that the degradation is not due to the adsorption of methylene blue on the $Ag/SiO_2/SrWO_4$ surface, rather to the photocatalytic degradation activity of $Ag@SiO_2/SrWO_4$.

The kinetic parameters of the degradation of MB by different catalysts were calculated based on the pseudo-first order reaction model. Degradation of MB by Ag/SiO_2, $SrWO_4$, and $Ag/SiO_2/SrWO_4$ and x%$Ag/SiO_2/SrWO_4$ was increased with time (C/C_0) (Fig. 6d and 7). The reaction rate constant (*k*) (Table 1) was calculated from the relation between the ln C/C_0 versus time (Fig. 7b and d). Catalytic degradation of MB in presence of H_2O_2 by Ag/SiO_2 was more than 8 times faster than $SrWO_4$. While the intimate contact in $Ag/SiO_2/SrWO_4$ boosted the rate constant more than 200 times than the pristine $SrWO_4$ and 25 time more than Ag/SiO_2. On the other hand, under visible light, the contact between Ag/SiO_2 and $SrWO_4$ increases the rate constant by 6.2 times than

Ag/SiO_2. Interestingly, the photodegradation under both visible light and H_2O_2 increases the rate constant 65.9 times than $SrWO_4$. Upon addition of 3.5%$Ag/SiO_2/SrWO_4$, the rate constant increases by 389 times than the pristine $SrWO_4$.

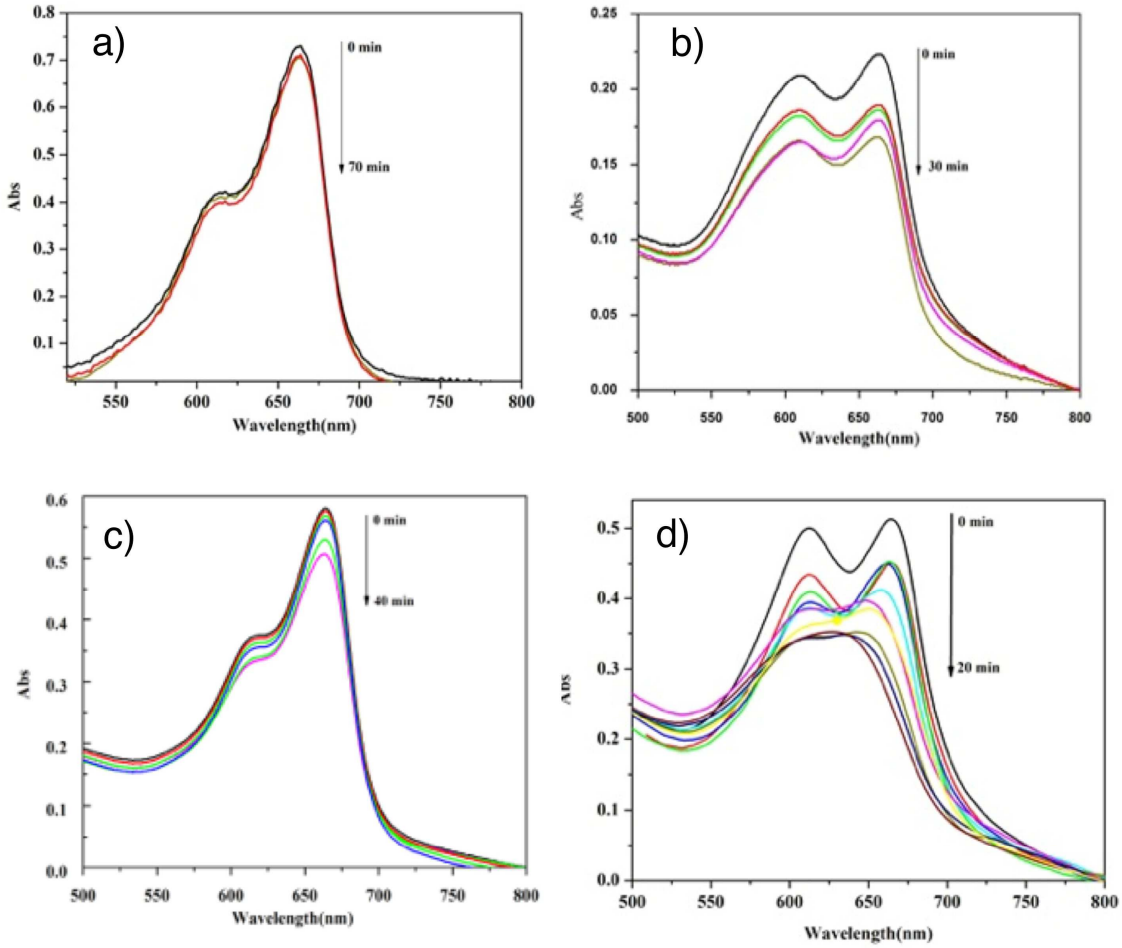

Fig. 4: Absorption spectrum of MB otodegredation under visible light for Ag/SiO_2, a) in the dark, b) in the dark and H_2O_2, c) visible light, d) visible light and H_2O_2.

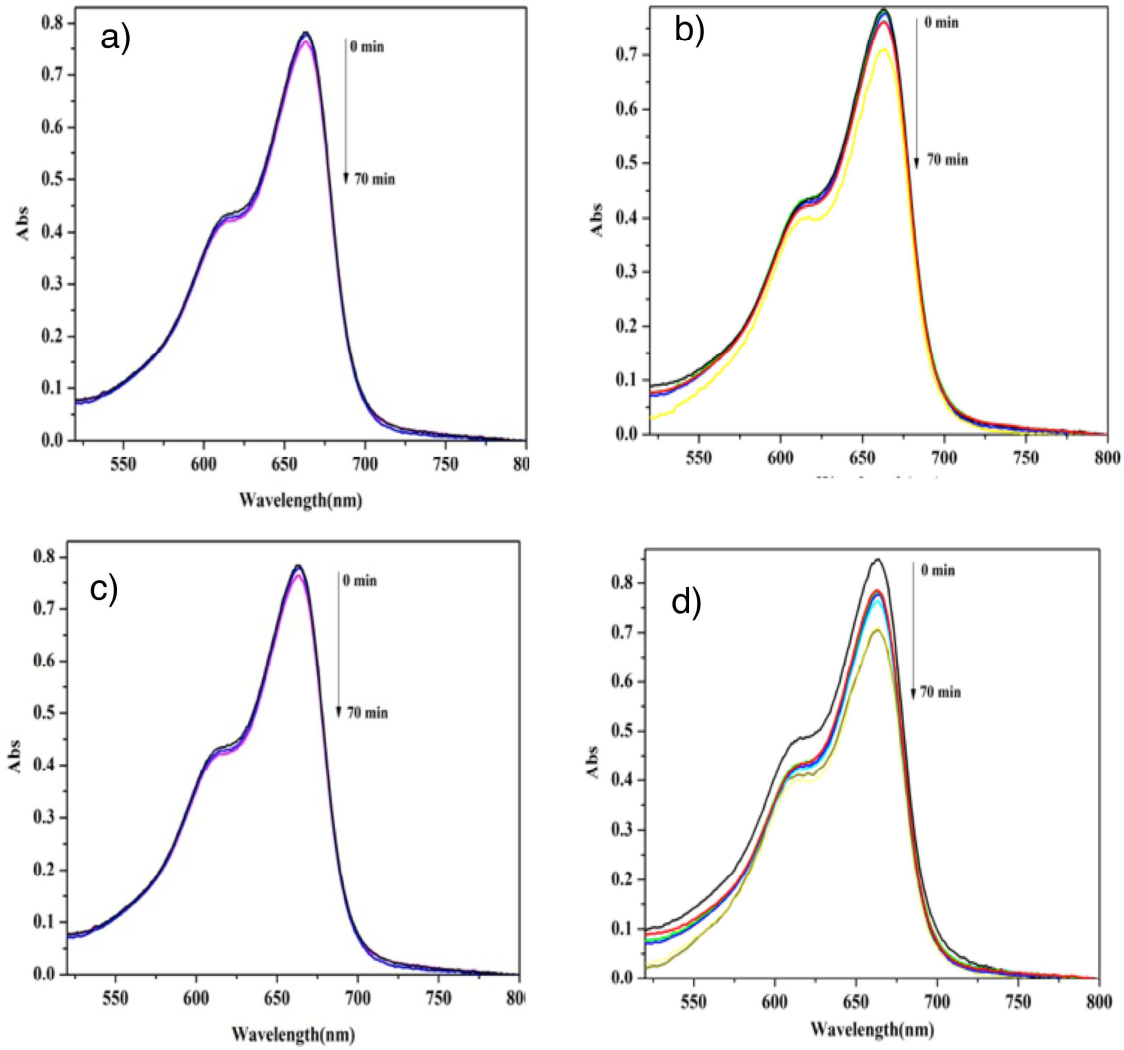

Fig. 5: Absorption spectrum of MB photodegradation under visible light for $SrWO_4$, a) in the dark, b) in the dark and H_2O_2, c) visible light, d) visible light and H_2O_2.

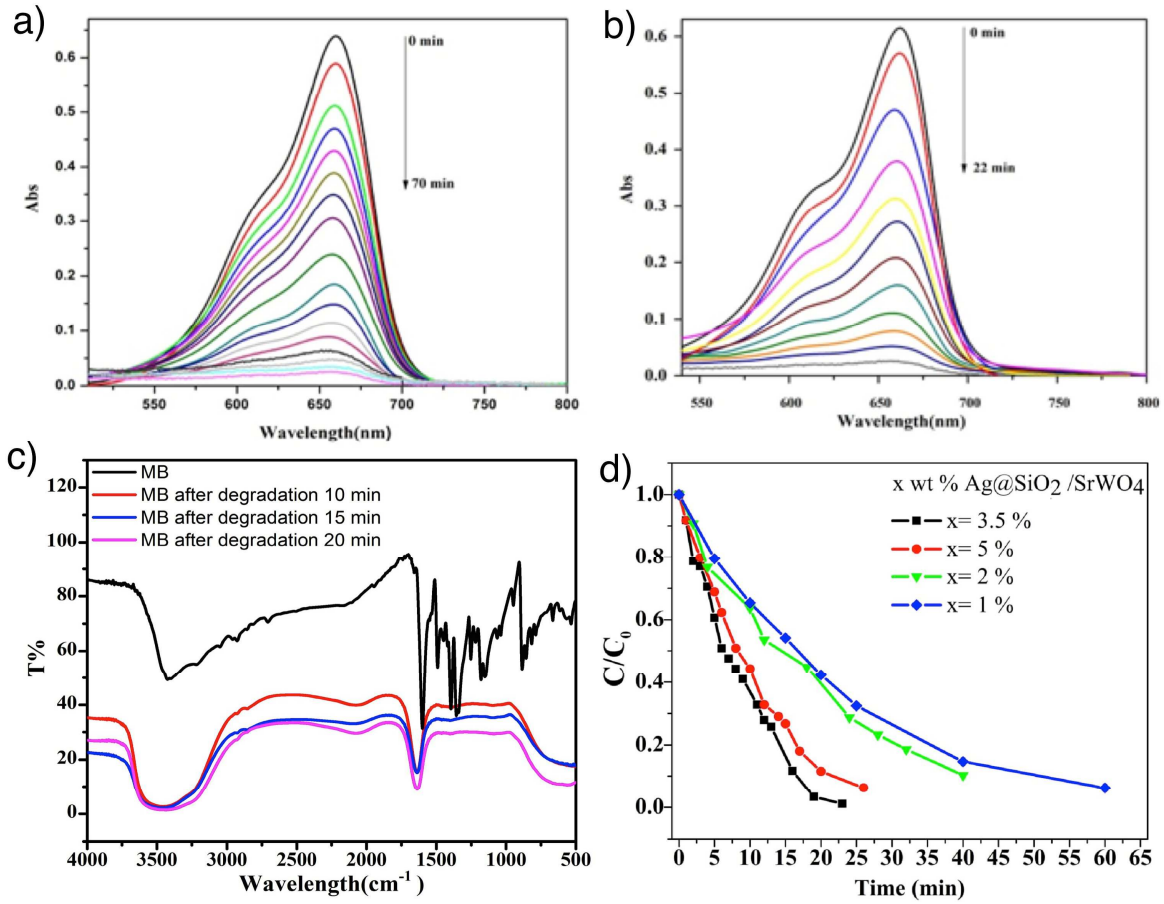

Fig. 6: Absorption spectrum of MB photodegradation under visible light for $Ag/SiO_2/SrWO_4$, a) visible light, b) visible light and H_2O_2, FT-IR of MB and $Ag/SiO_2/SrWO_4$ under different time irradiation c), and degradation of MB under different Ag NPs concentration d).

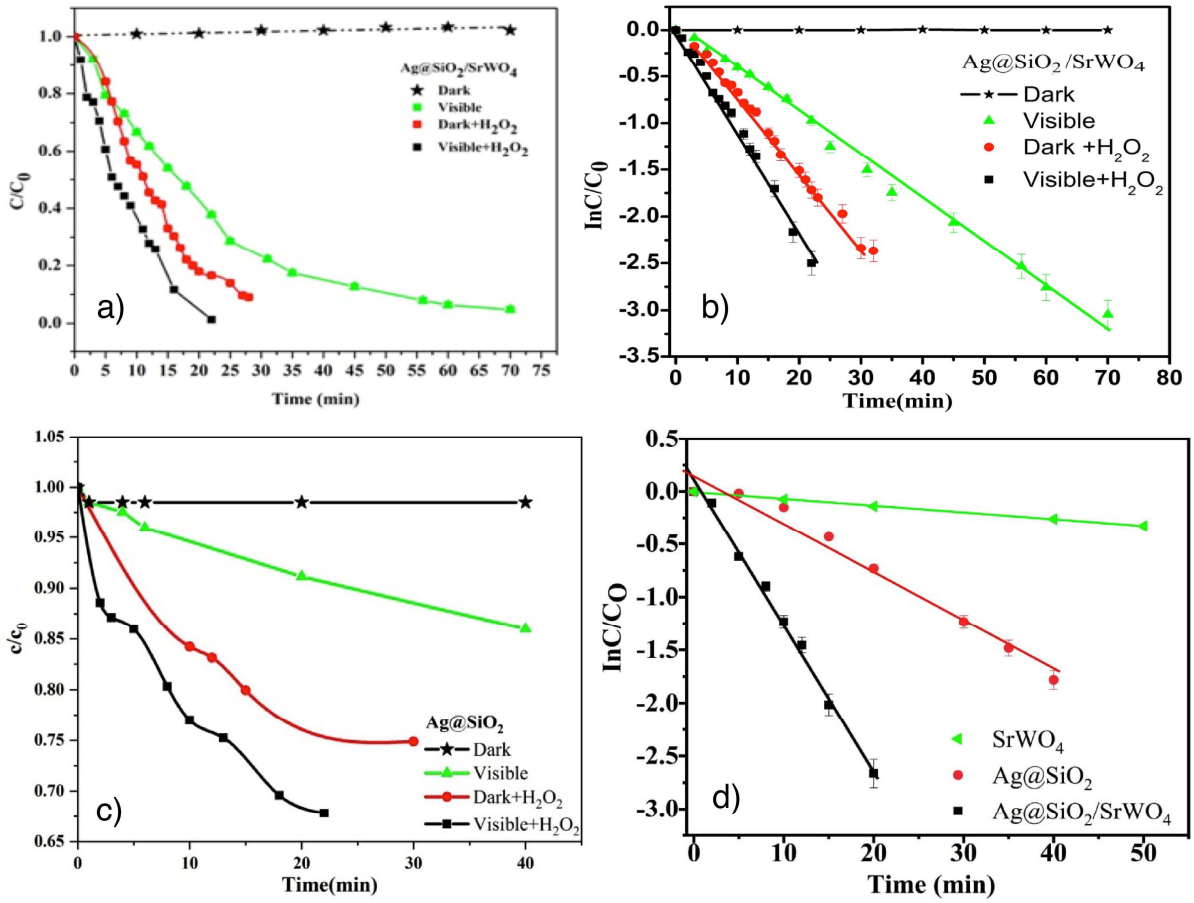

Fig. 7: Time profile (C/C_0 and lnC/C_0) for $Ag/SiO_2/SrWO_4$ and Ag/SiO_2

Table 1: kinetic parameters for the degradation of MB by $SrWO_4$, Ag/SiO_2, and $Ag/SiO_2/SrWO_4$.

Catalyst	Dark/H_2O_2 bond activation		Visible (plasmonic)		Visible/H_2O_2 Plasmonic/bond activation	
	k (10^{-4})	Time (min)	k (10^{-4})	Time (min)	k (10^{-4})	Time (min)
$SrWO_4$	3.9	50 (18)[a]	-	-	2.9	50 (18)
3.5%Ag/SiO_2	31.9	40 (28.8)	72.7	50 (15.2)	191	20 (38.8)
3.5%$Ag/SiO_2/SrWO_4$	788.9	35 (91)	457.1	70 (95.3)	1128	22 (99)

[a] Values in brackets gives the % of dye degradation

Effect of catalyst dose

In order to investigate the effect of the catalyst dose, different concentrations of $Ag/SiO_2/SrWO_4$ were used. Fig. 8a-c show the ability of different catalyst concentration to decompose the MB. The removal of MB was increased by increasing the catalyst dose from 10 mg (97% in 70 min) to 20 mg (99% in 20 min), while the removal percent was decreased with the increasing the dose to 30 mg (92.9% in 55 min), which attributed to aggregation of $Ag/SiO_2/SrWO_4$ at high catalyst dose. The nanoparticles aggregation reduces the active site and decreases the light penetration [38-40]. The kinetic rate constant was in the same direction with higher rate for 20 mg (0.1128 M^{-1}) and lowest rate constant in case of 30 mg (0.0489 M^{-1}) (Table 2). This result shows that the optimum catalyst concentration was 20 mg.

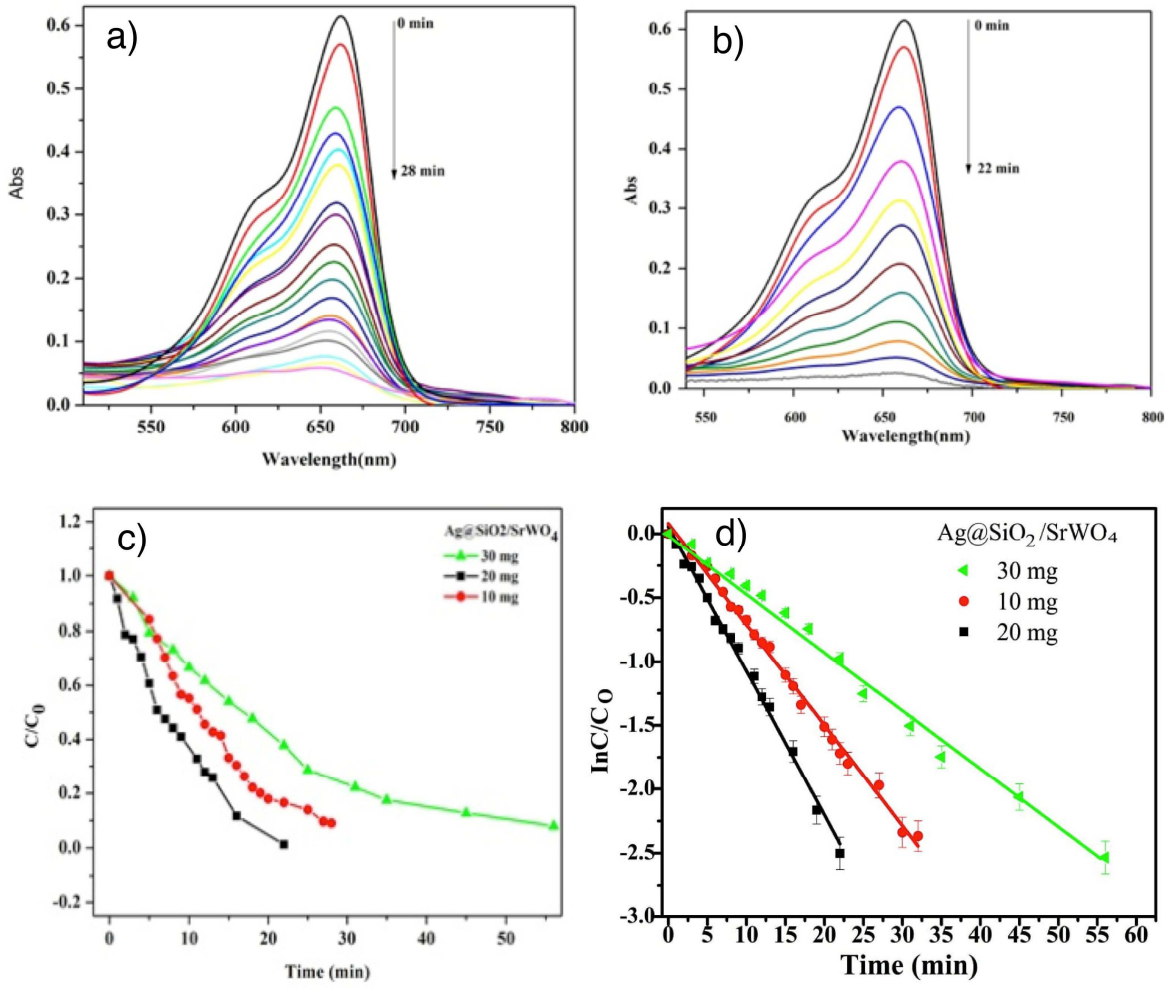

Fig. 8: Effect of $Ag/SiO_2/SrWO_4$ catalyst dose a) 10 mg, b) 20 mg and kinetic plots of different dose concentration.

Table 2: kinetic parameters for the degradation of MB by different doses of $Ag/SiO_2/SrWO_4$.

Parameters	3.5%$Ag/SiO_2/SrWO_4$		
	10 mg	**20 mg**	**30 mg**
k (10^{-4}) M^{-1}	803± 1.7	1128.8± 2.1	489.5± 1.26
Removal time, (%)	70 min (97.3)	22 min (99)	55 min (92.9)

Effect of pH

The pH effect on the photocatalytic activity of $Ag/SiO_2/SrWO_4$ was investigated (Fig. 9). The removal of MB was increased by increasing the pH from acidic (91% in 45 min) to neutral (97% in 19 min), and alkaline medium (97.9% in 15 min). The kinetic rate constant was in the same direction with higher rate in alkaline (0.1625 M^{-1}) and lowest rate in acidic medium (0.0552 M^{-1}) (Table 3). This result is in accordance with the $Ag/SiO_2/SrWO_4$ surface charge (Fig. 3b). The increased photocatalytic activity of $Ag/SiO_2/SrWO_4$ in alkaline medium was due to the electrostatic interaction between the positive MB and the negative charge on the nanocatalyst (–3.0 mV).

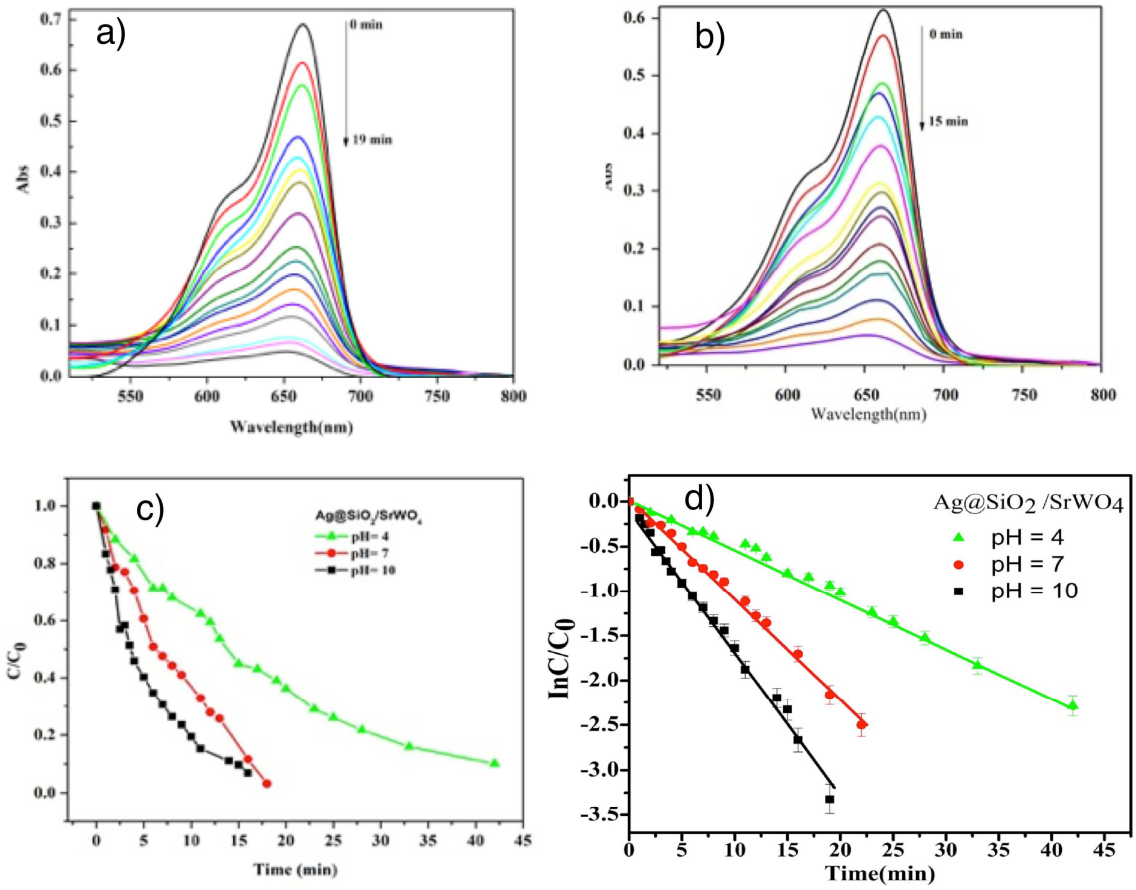

Fig. 9: Effect of pH on the photocatalytic activity of $Ag/SiO_2/SrWO_4$

Table 3: kinetic parameters for the degradation of MB by $Ag/SiO_2/SrWO_4$ at different pH.

Parameters	3.5%$Ag/SiO_2/SrWO_4$		
	pH 4	**pH 7**	**pH 10**
k (10^{-4}) M^{-1}	552.6	1128.8± 2.1	1625.1± 3.4
Removal time, (%)	45 min (91.0)	19 min (97%)	15 min (97.9%)

Reduction of *p*-nitrophenol by catalysts

The ability of the photocatalysts for the reduction of organic substrates was evaluated using *p*-nitrophenol (PNP) as organic model. The PNP absorption peak at 317 nm shifted to longer wavelength (400 nm) with the addition of $NaBH_4$ due to the formation of nitrophenolate ion [41-43]. With addition of the photocatalyst, the nitrophenolate peak at 400 nm gradually disappears in presence of simulated sunlight (Fig. 10a-b). In addition, the photocatalytic product *p*-aminophenol (PAP) posses a characteristic peak at 300 nm with the color solution change from pale-yellow to colorless [44]. The change in PNP concentration with time (C/C0) was calculated (Fig. 10c). The results reveal that the concentration of PNP slightly decreases with time after $SrWO_4$ (20 min, 20%), while in case of Ag/SiO_2 nanocatalyst, a significant decrease in PNP concentration was observed with time (40 min, 82%). On the other hand, dramatic decrease in time and increase in the rate constant was observed for $Ag/SiO_2/SrWO_4$ catalyst (20 min, 94%) (Fig. 10d). The kinetic rate constant was increased in the same direction for $SrWO_4$, Ag/SiO_2, and $Ag/SiO_2/SrWO_4$ which give values of 0.00413, 0.11573, 0.12289 $x10^{-4}$ M^{-1} respectively (Table 4).

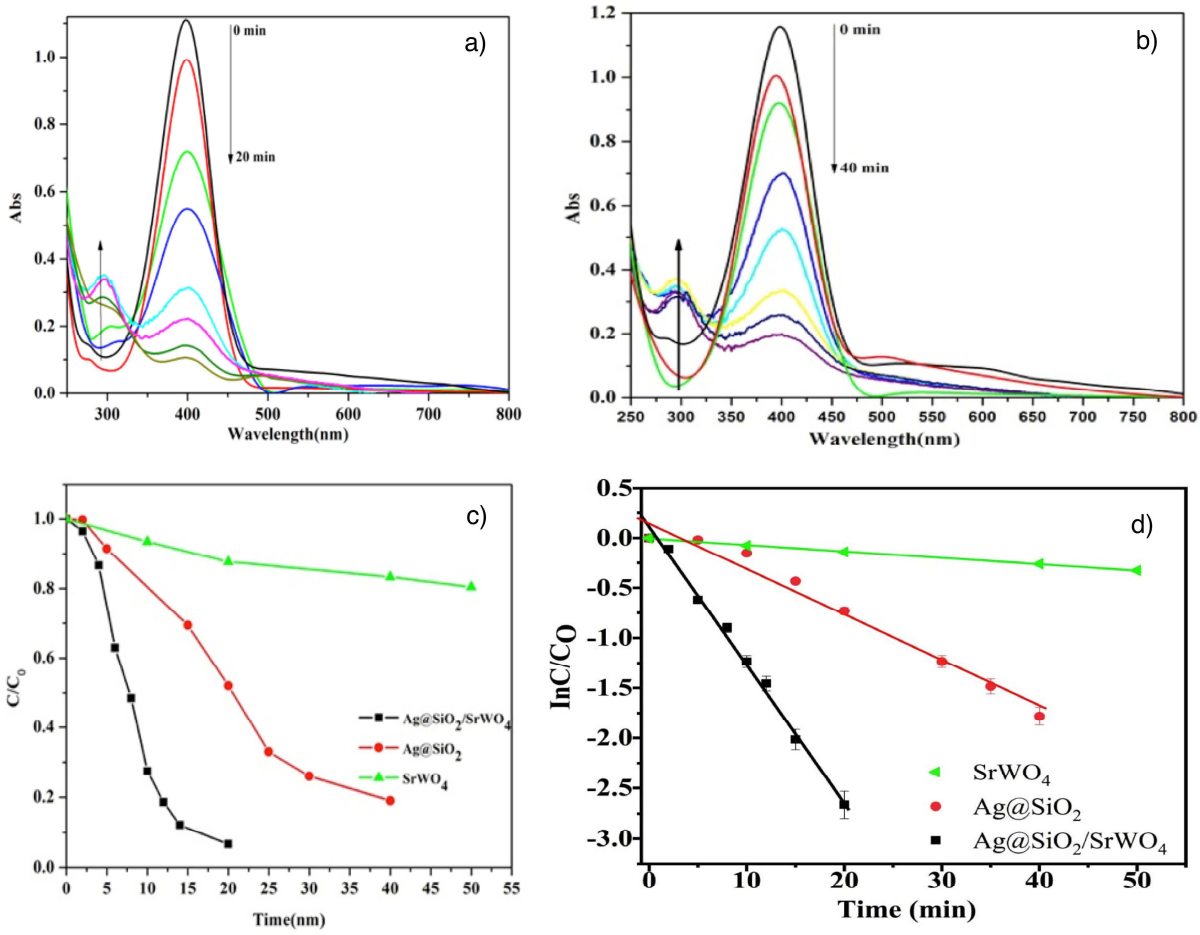

Fig. 10: a) UV absorption of time dependent *p*-NP to *p*-NA conversion under visible light using $Ag/SiO_2/SrWO_4$ and b) Ag/SiO_2, c) and d) are plots of C/C_0 versus reaction time and $\ln(C/C_0)$ versus reaction time.

To investigate the photocatalytic activity of $SrWO_4$, Ag/SiO_2 and $Ag/SiO_2/SrWO_4$, the photoluminescence prosperities were measured (Fig. 11a). Nanostructure show luminescence as a result of the recombination of the excited electron (e^{-}) with the hole (h^{+}); the increases of the recombination process gives high luminescence transition [45-48]. The photocatalytic activity of nanostructure will decrease accordingly; increase of the recombination decrease photocatalytic activity [49-51]. Here, the $SrWO_4$ show a strong photoluminescence peak at 360 nm and broad peak at 465 nm attributed to the high electron-hole recombination (Fig. 11a). Similarly, Ag/SiO_2 show high luminescence at 365 nm. The luminescence of $Ag/SiO_2/SrWO_4$ at 365 was lower than the Ag/SiO_2 and $SrWO_4$, which suggested that $Ag/SiO_2/SrWO_4$ more photocatalytic active.

Table 4: kinetic parameters for the reduction of *p*-NP to *p*-NA by $Ag/SiO_2/SrWO_4$, Ag/SiO_2, and $SrWO_4$.

Catalyst	k (10^{-4} M^{-1})	Percent (%)	Time (min)
$3.5\%Ag/SiO_2/SrWO_4$	0.12289	94.2	20
$3.5\%Ag/SiO_2$	0.11573	82	40
$SrWO_4$	0.00413	20	20

Catalytic and Photocatalytic mechanism

In order to investigate both catalytic and photocatalytic mechanism, trapping experiment for the reactive species was performed on the removal of MB by $Ag/SiO_2/SrWO_4$. We used trapping agents such as *p*-benzoquinone, isopropanol, and EDTA for $O_2^{-}\bullet$, $\bullet OH$, and h^+ respectively [52,53]. In the catalytic mechanism (dark), the removal of MB was significantly inhibited (91% in 35 min to 72.4% in 36 min) in presence of isopropanol, and from 91% to 63.9% by *p*-BQ. This result implies that the catalytic degradation of MB in presence of H_2O_2 dominated by the $\bullet OH$ and $O_2^{-}\bullet$ radicals (Fig. 13a). On the other hand, the photocatalytic mechanism was affected by the addition of different trapping agents. The addition of both isoprobanol and EDTA was slightly decreasing the reaction rate of MB removal, 25% and 10% respectively. While, addition of the same concentration of *p*-BQ to the reaction was significantly suppress the decoloration of MB (55.2%). These results show a significant role of the photogenerated electrons in the removal mechanism, while $\bullet OH$ and h^+ have a secondary role (Fig.13a).

Based on the trapping experiment, the catalytic degradation of MB by $Ag/SiO_2/SrWO_4$ through the adsorption and decomposition of H_2O_2 to active •OH and $O_2^{—}$• radical (Fig. 13b) [6,17,54]. The catalytic mechanism initiated by the adsorption of dye on the catalyst surface, where the adsorption percent was 11.2, 9.7, and 12.1 % for Ag/SiO_2, $SrWO_4$, and $Ag/SiO_2/SrWO_4$ respectively. Then, H_2O_2 decomposed on the surface by the Lewis acid and base surface equilibrium. The free electrons on the catalysts surface act as active centers for catalytic process [9,55]. This was confirmed by the negative surface charge of –25.0, –15.0, and –3.0 mV for $SrWO_4$, Ag/SiO_2 and $Ag/SiO_2/SrWO_4$ respectively. Alternatively, upon addition of H_2O_2 to $Ag/SiO_2/SrWO_4$, the surface Ag NPs oxidized to Ag^+, which activated the breakdown of H_2O_2 bond and generate the reactive $O_2^{—}$• radical (eq.1) [17,54]. Then the cycle was completed by further reformed Ag NPs through reduction of Ag^+ in presence of $O_2^{—}$• (eq. 2).

$$Ag\ NPs + H_2O_2 \rightarrow Ag^+ + O_2^{—}\bullet + H_2O \qquad (1)$$

$$Ag^+ + O_2^{—}\bullet \rightarrow Ag\ NPs \qquad (2)$$

This could be observed by the change in the FT-IR spectrum after H_2O_2 addition (Fig.12a) and confirmed by theoretical calculation. A new peak was observed after the addition of H_2O_2 to the nanocatalyst at 2100 $cm^{-1,}$ which attributed to the interaction between the surface Ag atoms and W atoms (Ag-W) [9]. In addition, the $Ag/SiO_2/SrWO_4$ XRD peaks intensity particularly at 25, 47, and 63^0 was decreases and slightly shifted after addition of 1mM H_2O_2 was observed (Fig. 12 b). In order to confirm the stability of the $Ag/SiO_2/SrWO_4$, the concentration of the Ag NPs were measured by the ICP-AES after the H_2O_2 injection to the solution. The result shows a slight decrease of the Ag NPs concentration (decreased from 3.5 to 3.25 %) after H_2O_2 addition, which might attribute to the dissolution of the Ag NPs. In order to investigate the nature of contacts in $Ag/SiO_2/SrWO_4$, DFT calculations (wb97x-

D/lanl2dz) were performed. The optimized structure of Ag_{14} clusters at the $SrWO_4$ unit cell shows a strong noncovalent interaction between Ag and W atoms (Fig 11b). The bond length of Ag…W ranged from 2.66 to 2.78 Å, which is less than the sum of the van der walls radius. The $SrWO_4$•Ag complex was stabilized by 4.67 kcal/mole.

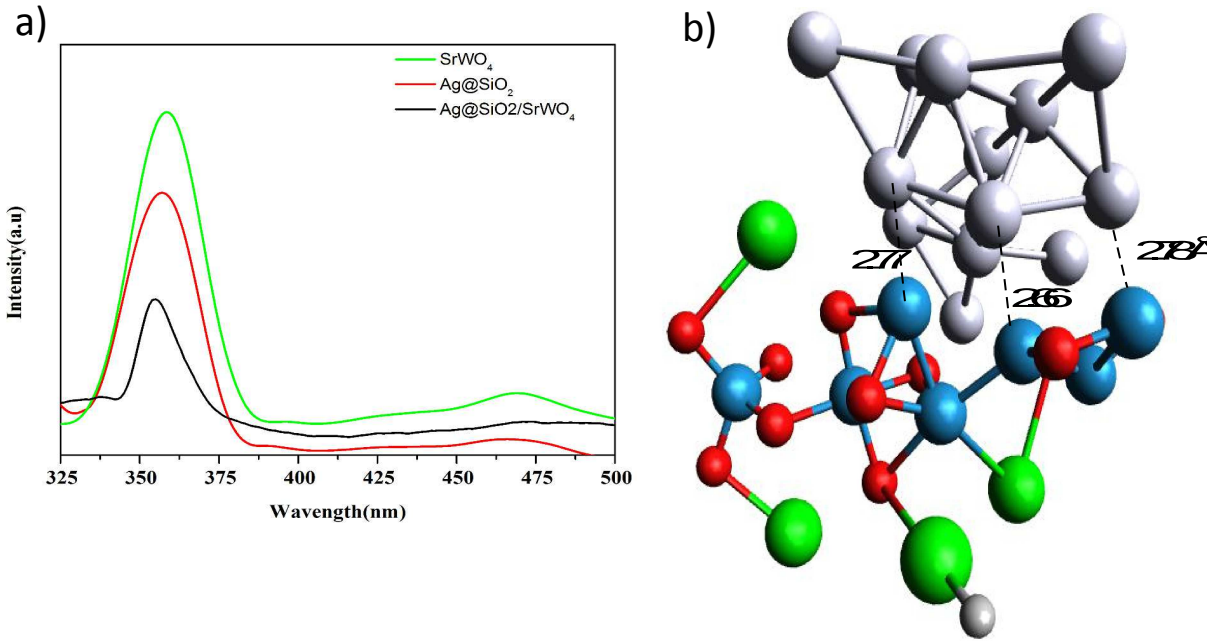

Fig. 11: a) Photoluminescence of $SrWO_4$, Ag/SiO_2, and $SrWO_4$, b) optimized structure of $Ag14/SrWO_4$ at wb97x-D/lanl2dz.

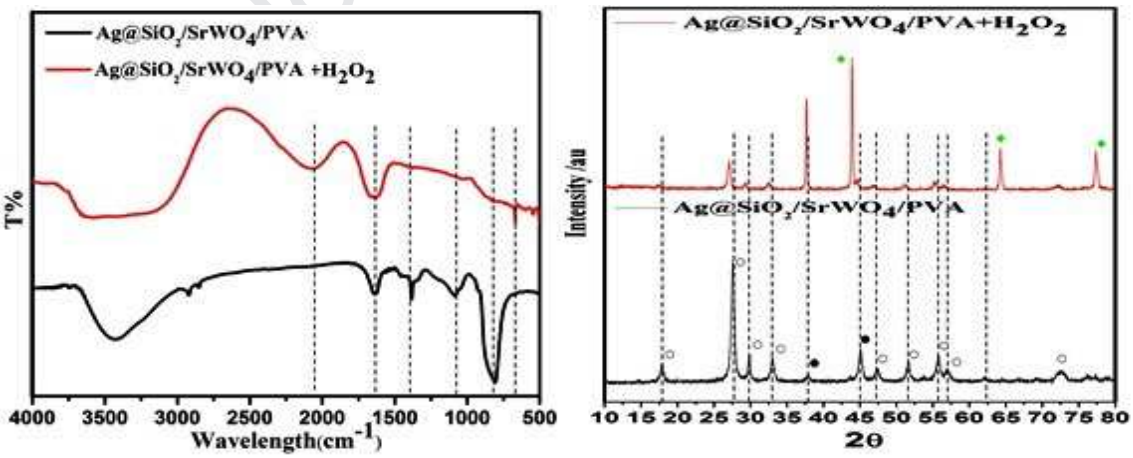

Fig. 12: a) FTIR and b) XRD spectrum of $Ag/SiO_2/SrWO_4$ after H_2O_2 treatment (1 mM).

Under visible light, $SrWO_4$ absorption was neglected due to the wide band gap (3.8 eV)[14], which highly restricted its use as photocatalyst under visible light. To increase visible light absorption, plasmonic noble metals such as Ag NPs were doped in order to enhance the photocatalytic process [53,56-58]. To asses the photocatalytic mechanism, CB and VB potentials for both $SrWO_4$ and Ag/SiO_2 catalysts were calculated according to the formula [59]:

$$E_{CB} = \chi - E^e - 0.5\, E_g \quad (1)$$

$$E_{VB} = E_{CB} + E_g \quad (2)$$

The E_{CB}, and E_{VB}, are the conduction and valence band potential energy, E^e is the energy of free electrons against standard hydrogen electrode (4.5 eV) [60]. On the other hand, χ is the electronegativity of the individual semiconductors and calculated by Eq. 3 [61]:

$$\chi = [\chi(A)^a \chi(B)^b \chi(C)^c]^{1/(a+b+c)} \quad (3)$$

where, a, b and c are the number of the individual atoms in semiconductors. For $SrWO_4$, the potential for CB and VB was calculated as -0.88 and 3.52 eV respectively. On the other hand, the calculated CB and VB potentials for Ag/SiO_2 catalyst were -0.45 and 3.21 eV respectively. The charge separation mechanism propose that the separated electrons on the $SrWO_4$ CB will be injected to the Ag/SiO_2 CB as the former has more negative potential. Consequently, the accumulated holes in the Ag/SiO_2 VB will transferred to the $SrWO_4$ VB to form an n-p heterojunction (Fig. 14a). However, this mechanism is abandoned by the lake of visible light absorption by $SrWO_4$ to generate electron/hole separation due to the high band gap (3.8 eV) [14]. Alternatively, plasmonic Ag NPs decorated SiO_2 NPs forms surface SPR through the interactions of electromagnetic radiation with the surface free electrons (Fig.14b) [62-64]. The resulting high kinetic electrons (hot electrons) were injected to the CB of $SrWO_4$. The hot electrons on $SrWO_4$ CB react with the surface O_2 to generate the active

superoxide radicals ($O_2^{-\bullet}$) radical, sequentially, electron holes (h^+) accumulated on the Ag/SiO_2 VB. Generation of reactive oxygen species ($O_2^{-\bullet}$ and h^+) boosted the MB photo-oxidation and *p*-nitrophenol reduction.

Addition of H_2O_2 to the photocatalytic reaction (Table 1) increases the $Ag/SiO_2/SrWO_4$ photocatalytic activity. This increase attributed to excess reactive oxygen species ($O_2^{-\bullet}$ and h^+) liberated form the external H_2O_2 [65].

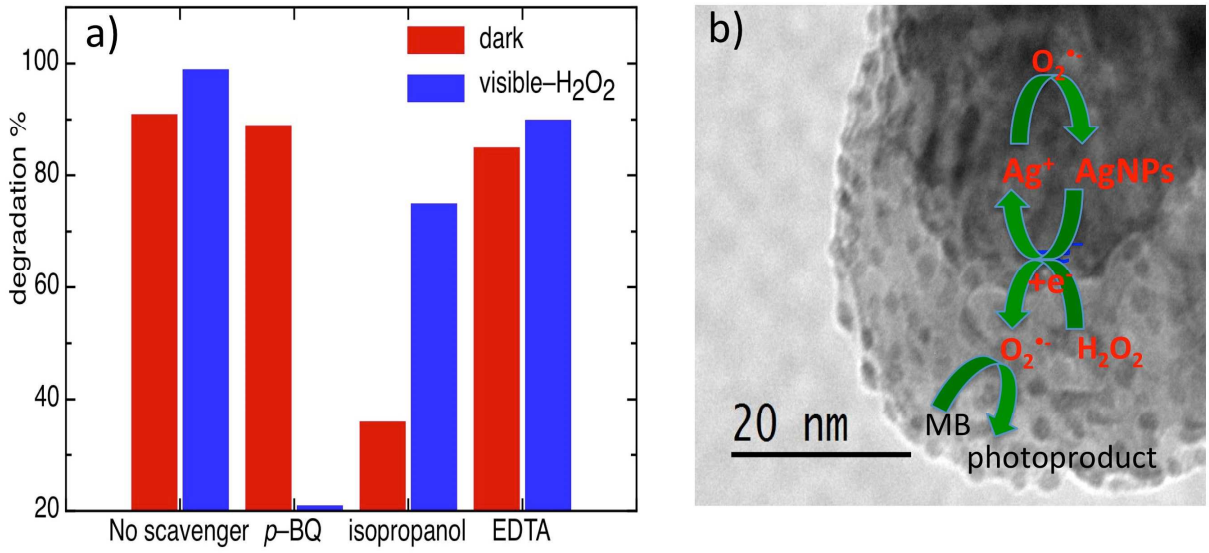

Fig. 13: a) trapping agents effect on the degradation of MB by $Ag/SiO_2/SrWO_4$ under visible light, b) Catalytic mechanism of the removal of MB by $Ag/SiO_2/SrWO_4$.

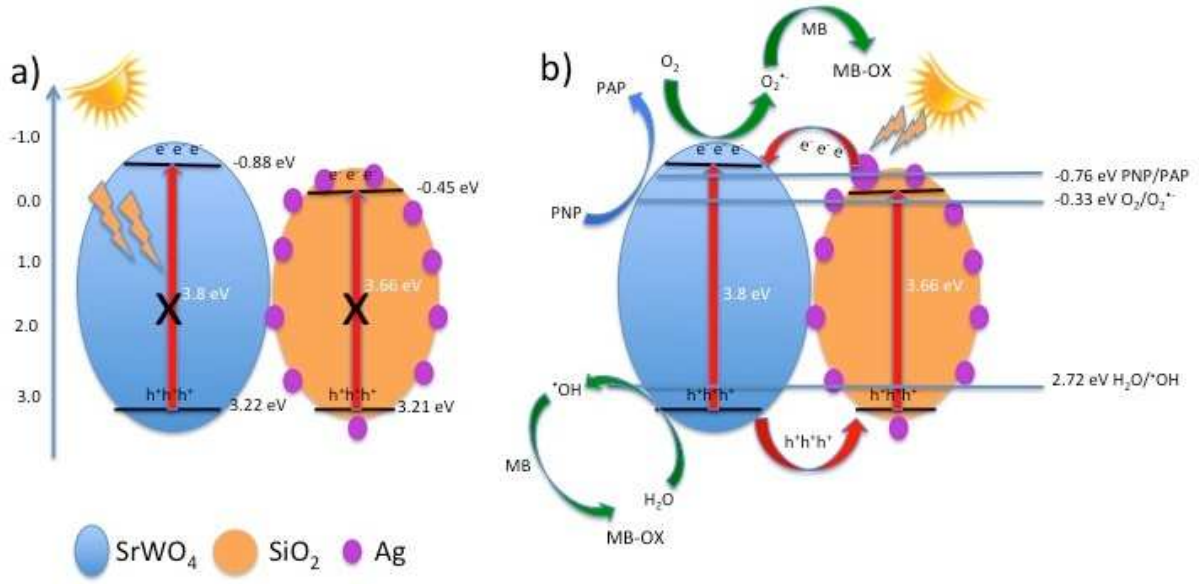

Fig. 14: photocatalytic mechanism for the proposed n-p heterojunction (a), and the plasmon enhanced photocatalytic (b) under simulated sunlight.

Photocatalyst stability

The stability of the photocatalyst is an important factor for practical application. In order to evaluate the stability, after each experiment the photocatalyst was centrifuged, collected and dried for the next cycle. Fig. 15 shows the successive 5 cycles activity of the MB photodegradation over $Ag/SiO_2/SrWO_4$ under visible light. The photocatalytic efficiency of $Ag/SiO_2/SrWO_4$ shows more than 80% form the initial degradation after 5 cycles. The decrease in the photocatalytic efficiency attributed to the dissolution of Ag NPs, the ICP results confirmed the slight change of Ag NPs concentration from 3.5% to 3.25%). This results show that $Ag/SiO_2/SrWO_4$ is stable and durable photocatalyst. In addition, the $Ag/SiO_2/SrWO_4$ photocatalyst show superior performance compared to the corresponding $SrWO_4$ and $SrWO_4$ doped materials (Table 5). The optical absorption of $SrWO_4$ in the UV region (280 nm) restricts its applications in photocatalysis. As a result, the usage of $SrWO_4$ without doping takes long time to degrade the organic dyes. Moreover, when $SrWO_4$ doped with Eu^{+3} or graphene nanosheets, the performance of the photocatalyst was not significantly

improved. On the other hand, when $SrWO_4$ doped with 3.5% of Ag NPs supported on SiO_2, the photocatalytic performance was significantly improved after irradiation with visible light (Table 5). This result show that posses high stability (used several times) and superior performance (short time under visible light) for the photocatalytic degradation of organic dyes (MB) at different environment.

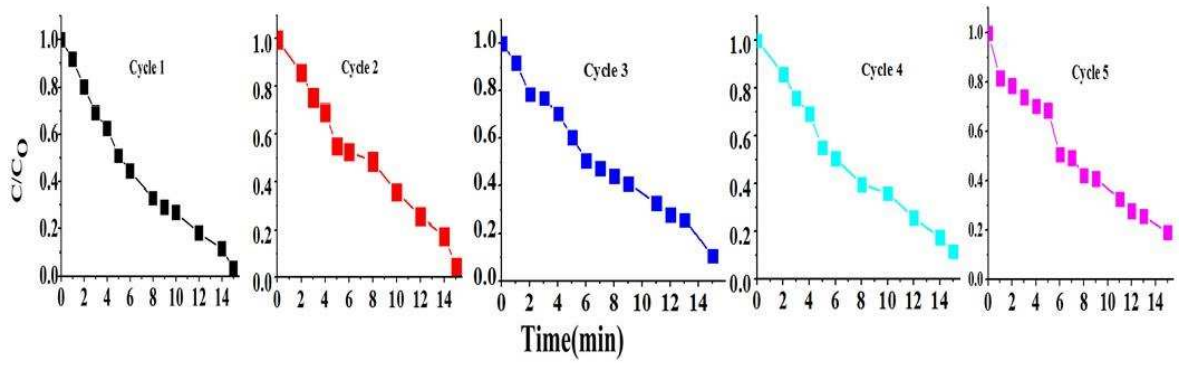

Fig. 15: Stability of $Ag/SiO_2/SrWO_4$ under visible light irradiation for MB aqueous solution.

Table 5: photocatalytic activity of different $SrWO_4$ catalysts.

Photocatalyst	Light irradiation	Target dye	pH	Decomposition (%)	Time (min)	Ref.
$SrWO_4$	UV	MB	7	54	60	[15]
	UV		3	74	60	
$SrWO_4$	UV	RhB		100	80	[66]
	UV	Rh6G		100	50	
$SrWO_4$	UV	MO	6.9	29	110	[67]
	UV	MO	3.1	82	30	
$Srwo_4$	Visible	RhB		80	240	[68]
$Srwo_4/Eu^{+3}$	Visible	MB		82	120	[16]
$Srwo_4$	UV	MO		57.3	110	[69]
$Srwo_4/4\%GO$	UV	MO		95.7	110	

3.5%Ag/SiO_2/$SrWO_4$	Visible	MB	10	97.9	15	This work

Conclusion

Activated H_2O_2 on Ag/SiO_2/$SrWO_4$ surface enhance the catalytic and photocatalytic removal of both MB and *p*-nitrophenol at wide pH values. The enhanced catalytic activity was assigned to the specific interaction between surface Ag NPs and the W atoms in $SrWO_4$. On another hand, the photocatalytic activity was attributed to the injection of the Ag NPs hot electrons to the $SrWO_4$ CB. Ag/SiO_2/$SrWO_4$ show enhanced catalytic and photocatalytic activity towards removal of organic pollutants at wide pH values and minimum dose.

Acknowledgment

The authors acknowledge the financial support from Kafrelsheikh University. H.S.El-Sheshtawy acknowledges the computation time at Jacobs University Bremen.

References

[1] T. Kanagaraj, S. Thiripuranthagan, Appl. Catal. B: Environ. 207 (2017) 218.
[2] M. Bourgin, E. Borowska, J. Helbing, J. Hollender, H. P. Kaiser, C. Kienle, C. S. McArdell, E. Simon, U. von Gunten, Water Res. 122 (2017) 234.
[3] L. Lyu, L. Zhang, G. He, H. He, C. Hu, J. Mater. Chem. A 5 (2017) 7153.
[4] A.D. Bokare, W. Choi, J. Hazard. Mater. 275 (2014) 121.
[5] D. Yuan, C. Zhang, S. Tang, X. Li, J. Tang, Y. Rao, Z. Wang, Q. Zhang, Water Res. 163 (2019) 114861.
[6] C. Ma, S. Feng, J. Zhou, R. Chen, Y. Wei, H. Liu, S. Wang, Appl. Catal. B: Environ. 259 (2019) 118015.
[7] K. Shoueir, H. El-Sheshtawy, M. Misbah, H. El-Hosainy, I. El-Mehasseb, M. El-Kemary, Carbohydr. Polym. 197 (2018) 17.
[8] J. Ma, Q. Yang, Y. Wen, W. Liu, Appl. Catal. B: Environ. 201 (2017) 232.
[9] X. Wang, D. Li, Z. Nan, Sep. Purif. Technol. 224 (2019) 152.
[10] J. Ding, Q. Zhong, S. Zhang, F. Song, Y. Bu, Chem. Eng. J. 243 (2014) 176.
[11] H. Farsi, Z. Barzgari, Int. J. Nanosci. 13 (2014) 1450013.
[12] S. Vidya, S. Solomon, J.K. Thomas, J. Mater. Sci. Mater. Electron. 25 (2014) 693.
[13] L.S. Cavalcante, J.C. Sczancoski, N.C. Batista, E. Longo, J.A. Varela, M.O. Orlandi, Adv. Powder Technol. 24 (2013) 344.
[14] X. Liu, Y. Nie, H. Yang, S. Sun, Y. Chen, T. Yang, S. Lin, Solid State Sci. 55 (2016) 130.
[15] C. Shivakumara, R. Saraf, S. Behera, N. Dhananjaya, H. Nagabhushana, Mater. Res. Bull. 61 (2015) 422.

[16] Y. Zheng, J. Lin, Q. Wang, Photochem. Photobiol. Sci. 11 (2012) 1567.
[17] D. He, S. Garg, T.D. Waite, Langmuir 28 (2012) 10266.
[18] A.M. Jones, S. Garg, D. He, A.N. Pham, T.D. Waite, Environ. Sci. Technol. 45 (2011) 1428.
[19] A. Nel, T. Xia, L. Madler, N. Li, Science 311 (2006) 622.
[20] J.R. Morones, J.L. Elechiguerra, A. Camacho, K. Holt, J.B. Kouri, J.T. Ramirez, M.J. Yacaman, Nanotechnology 16 (2005) 2346–2353.
[21] E. Mendis, N. Rajapakse, H.G. Byun, S.K. Kim, Life Sci. 77 (2005) 2166–2178.
[22] Y.H. Kim, D.K. Lee, H.G. Cha, C.W. Kim, Y.S. Kang, J. Phys. Chem. C 111 (2007) 3629.
[23] A. Barhoum, M. Rehan, H. Rahier, M. Bechelany, G. Van Assche, ACS Appl. Mater. 8 (2016) 10551.
[24] D. He, M. Kacopieros, A. Ikeda-Ohno, T.D. Waite, Environ. Sci. Technol. 48 (2014) 12320.
[25] I. Pastoriza-Santos, L.M. Liz-Marzán, Nano Letters 2 (2002) 903.
[26] L. Mulfinger, S.D. Solomon, M. Bahadory, A.V. Jeyarajasingam, S.A. Rutkowsky, C. Boritz, Journal of Chemical Education 84 (2007) 322.
[27] C. Graf, D.L.J. Vossen, A. Imhof, A. van Blaaderen, Langmuir 19 (2003) 6693.
[28] T.-H. Liou, F.-W. Chang, J.-J. Lo, Ind. Eng. Chem. Res. 36 (1997) 568.
[29] F. Wang, G. Li, Q. Zhou, J. Zheng, C. Yang, Q. Wang, Appl. Surf. Sci. 425 (2017) 180.
[30] Q. Chen, M. Zhang, J. Li, G. Zhang, Y. Xin, C. Chai, Chem. Eng. J. 389 (2020) 124476.
[31] M. Nawaz, A. Shahzad, K. Tahir, J. Kim, M. Moztahida, J. Jang, M.B. Alam, S.-H. Lee, H.-Y. Jung, D.S. Lee, Chem. Eng. J. 382 (2020) 123053.
[32] A. Houas, H. Lachheb, M. Ksibi, E. Elaloui, C. Guillard, J.-M. Herrmann, Appl. Catal. B Environ. 31 (2001) 145.
[33] Q. Zhang, C. Li, T. Li, Int. j. photoenergy 2012 (2012) 398787.
[34] Y.-H. Wu, T. Wu, Y.-W. Lin, Mater. Res. Bull. 118 (2019) 110500.
[35] Y. Ahmed, Z. Yaakob, P. Akhtar, Catal. Sci. Technol. 6 (2016) 1222.
[36] P. Xu, T. Xu, J. Lu, S. Gao, N.S. Hosmane, B. Huang, Y. Dai, Y. Wang, Energy Environ. Sci. 3 (2010) 1128.
[37] S. Lee, K.-S. Lee, S. Sorcar, A. Razzaq, C. Grimes, S.-I. In, J. Photochem. Photobiol. A (2017).
[38] M. Gholami, M. Shirzad-Siboni, M. Farzadkia, J.-K. Yang, Desalin. Water Treat. 57 (2016) 13632.
[39] R. Tanwar, U.K. Mandal, RSC Advances 9 (2019) 8977.
[40] R. Kumar, J. Rashid, M.A. Barakat, Colloid Interfac. Sci. 5 (2015) 1.
[41] Y. Fu, T. Huang, J.Z. B. Jia, X. Wang, Appl. Catal. B: Environ. 202 (2017) 430.
[42] K. Singh, D. Kukkar, R. Singh, P. Kukkar, N. Bajaj, J. Singh, M. Rawat, A. Kumar, K.-H. Kim, J. Ind. Eng. Chem. 81 (2020) 196.
[43] J. Wu, J. Wang, T. Wang, L. Sun, Y. Du, Y. Li, H. Li, Appl. Surf. Sci. 466 (2019) 342.
[44] Y. Wang, Q. Li, P. Zhang, D. O'Connor, R.S. Varma, M. Yu, D. Hou, J. Colloid Interface Sci. 539 (2019) 161.
[45] V. Nguyen, J. Si, L. Yan, X. Hou, Carbon 95 (2015) 659.
[46] M. O'Neil, J. Marohn, G. McLendon, J. Phys. Chem.A 94 (1990) 4356.
[47] D. Shi, Z. Xiong, J. Li, B.Q. Luo, L.M. Fang, Y.H. Xia, Z. Gao, Mater. Res. Express 6 (2019) 105021.
[48] H. Zhang, J. Liu, C. Wang, G.S. Selopal, D. Barba, Z.M. Wang, S. Sun, H. Zhao, F. Rosei, ACS Photonics 6 (2019) 2421.
[49] N. Xuan Sang, N. Minh Quan, N. Huu Tho, N. Tri Tuan, T. Thanh Tung, Semicond. Sci. Technol. 34 (2019) 025013.
[50] X. Zhou, C. Shao, S. Yang, X. Li, X. Guo, X. Wang, X. Li, Y. Liu, ACS Sustain. Chem. Eng. 6 (2018) 2316.
[51] T.K. Le, M. Kang, V.T. Tran, S.W. Kim, Mater. Sci. Semicond. Process. 100 (2019) 159.
[52] W. Cui, J. He, H. Wang, J. Hu, L. Liu, Y. Liang, Appl. Catal. B: Environ. 232 (2018) 232.
[53] H.S. El-Sheshtawy, H.M. El-Hosainy, K.R. Shouir, I.M. El-Mehasseb, M. El-Kemary, Appl. Surf. Sci. (2019) 268.
[54] H. Rong, S. Garg, T.D. Waite, Environmental Science & Technology 53 (2019) 6688.

[55] V.P. Santos, M.F.R. Pereira, P.C.C. Faria, J.J.M. Órfão, Journal of Hazardous Materials 162 (2009) 736.
[56] L. Chen, R. Chen, H. Hu, G. Li, Mater. Lett. 242 (2019) 47.
[57] O.A. Krysiak, P.J. Barczuk, K. Bienkowski, T. Wojciechowski, J. Augustynski, Catal. Today 321-322 (2019) 52.
[58] M.M. Ibrahim, A. Mezni, H.S. El-Sheshtawy, A.A. Abu Zaid, M. Alsawat, N. El-Shafi, S.I. Ahmed, A.A. Shaltout, M.A. Amin, T. Kumeria, T. Altalhi, Appl. Surf. Sci. 479 (2019) 953.
[59] L. Zhang, X. Wang, Q. Nong, H. Lin, B. Teng, Y. Zhang, L. Zhao, T. Wu, Y. He, Appl. Surf. Sci. 329 (2015) 143.
[60] S.R. Morrison, Electrochemistry at Semiconductor and Oxidized Metal

Electrode, Plenum, New York, 1980.
[61] Q. Yuan, L. Chen, M. Xiong, J. He, S.L. Luo, C.T. Au, S.F. Yin, Chem.

Eng. J. 255 (2014) 394.
[62] N. Güy, M. Özacar, J. Photoch Photobio. A 370 (2019) 1.
[63] L. Zhang, C. Liang, H. Guo, C.-G. Niu, X.-F. Zhao, X.-J. Wen, G.-M. Zeng, Nanoscale 11 (2019) 6662.
[64] D.K. Bhatt, U.D. Patel, J. Phys. Chem. Solids 135 (2019) 109118.
[65] T. Wen, H. Zhang, Y. Chong, W.G. Wamer, J.-J. Yin, X. Wu, Nano Research 9 (2016) 1663.
[66] L.S. Cavalcante, J.C. Sczancoski, N.C. Batista, E. Longo, J.A. Varela, M.O. Orlandi, Ad. Powder Technol. 24 (2013) 344.
[67] Z. Shan, Y. Wang, H. Ding, F. Huang, J. Mol. Catal. A 302 (2009) 54.
[68] H. Hossainian, M. Salavati-Niasari, M. Bazarganipour, J. Mol. Liq. 220 (2016) 747.
[69] X. Liu, Y. Nie, H. Yang, S. Sun, Y. Chen, T. Yang, S. Lin, Solid State Sciences 55 (2016) 130.

Highlights

- Facile synthesis of $Ag@SiO_2$ on $SrWO_4$ surface.
- H_2O_2 activated on $Ag@SiO_2/SrWO_4$ surface in the dark and under visible light.
- Both catalytic and photocatalytic enhanced in presence of H_2O_2 at wide pH range
- Unique contact between Ag and W activated H_2O_2 in the dark, while plasmonic nanoparticles was the main source of ROS.

Conflict of interest: the authors declare no conflict of interest